ADVANCED ELECTRONIC MATERIALS
www.advelectronicmat.de

Fabrication of High Specific Electrical Conductivity and High Ampacity Carbon Nanotube/Copper Composite Wires

Mohamed B. Bazbouz, Atif Aziz, Davor Copic, Michael De Volder, and Mark E. Welland*

A challenge is to integrate Cu with carbon nanotubes (CNTs) and form a free-standing composite wire. This is achieved by first making a CNT filament using high concentration (20 g L^{-1}) CNT dispersion, an acid-free wet spinning process and then by replacing the polymer with copper using heat based polymer decomposition and periodic pulse reverse electroplating. It is demonstrated that indeed the specific conductivity and the current-carrying capability (or ampacity) are increased manifold. The multiwalled CNT (MWCNT)/Cu composite wires developed in this paper have electrical conductivity $\sigma \approx 5.5 \times 10\ 5$ S cm^{-1}. These MWCNT/Cu wires are 2/3rd the weight of bulk Cu wires. Their specific electrical conductivity is $\sigma_\rho \approx 9.38 \times 10\ 4$ S $cm^2\ g^{-1}$ which is 45% higher than International Annealed Copper Standard Cu. These composite wires have an ampacity of $A \approx 20 \times 10^5$ and 4×10^5 A cm^{-2} for 1.5 and 17 mm gauge length wires, respectively, which is four to six times higher than pure Cu depending on the wire lengths. MWCNTs volume percentage in the MWCNT/Cu wire is about 40%.

1. Introduction

Copper (Cu) is one of the most abundant and commonly used conducting metal, it has a very good electrical conductivity (EC) of $\sigma = 5.96 \times 10^5$ S cm^{-1}, but it is heavy (density 8.96 g cm^{-3}) and has a specific electrical conductivity (SEC) of 6.6×10^4 S cm g^{-1} at room temperature.[1,2] Aluminum (Al) on the other hand has high SEC of 13.96×10^4 S cm g^{-1}, but its EC of 3.77×10^5 S cm^{-1} is much lower than copper.[3] Ampacity or the current carrying capacity of Al is also many times less than copper.[4] For making next generation of conducting cables, high electrical conductivity is desirable for suppressing Joule heating and at the same time high specific electrical conductivity is essential for reducing weight. Especially for aerospace industry and electric motors, these wires and cable can have a very big impact by reducing CO_2 emission and enhancing the efficiency of motors, power cables and transformers. Carbon nanotubes (CNTs) have emerged as a possible candidate for achieving the above mentioned properties.[5] Individual CNTs have been demonstrated to have very high EC of 0.35×10^5 and 10×10^5 S cm^{-1} for multiwalled (MW) and single walled (SW) carbon nanotubes, respectively[6] and thus SEC of 2×10^4 and 62.5×10^4 S cm g^{-1} for MWCNTs and SWCNTs, respectively[7] and ampacity of 4×10^9 A cm^{-2} for SWCNTs.[8] However, when CNTs are combined to form a useable wire, these properties drop many order of magnitude.[9] Over the last decade there has been a great progress in creating CNTs wires using wet spinning (spinning using super-acids[10–13] and surfactant-based coagulation spinning[14–31]) and dry spinning (aligned forest-array spinning[32–54] and direct spinning of CNTs aerogel[40,55–87]). Good quality CNTs wires are now commercially available.[88] However, electrical conductivity and the specific electrical conductivity of these CNTs wires are still less than copper.[89–93] Carbon nanotubes/copper (CNTs/Cu) composite is also a very promising candidate for making light weight wires. It has been demonstrated by using a lithographically defined small scale wires deposited on a silicon chip that CNTs/Cu composite wires can have an ampacity 100 times more than copper and have an SEC of 9×10^4 S cm g^{-1}.[94] This study shows that CNTs/Cu composite wires can have a specific electrical conductivity greater than copper but achieving such properties for a free standing and continuous wire still remains a challenge.

Achieving a uniform dispersion of CNTs in a copper matrix is a primary requirement for making CNTs/Cu composite wires. In this paper we have adopted a new method for making CNTs/Cu composite wires and we have been successful in making free standing CNTs/Cu composite wires which have a specific electrical conductivity and ampacity greater than copper. To achieve this, a microfluidization (MF) dispersion process has been developed for creating very high concentration (up to 20 mg mL^{-1}) CNTs dispersion using carboxymethyl cellulose sodium salt (Na-CMC) as a surfactant and water. This high viscosity dispersion has been converted into CNTs filaments using an acid free wet spinning process. Na-CMC polymer is then decomposed and

Dr. M. B. Bazbouz, Dr. A. Aziz, Prof. M. E. Welland
The Nanoscience Centre
Department of Engineering
University of Cambridge
Cambridge CB3 0FF, UK
E-mail: mbb40@cam.ac.uk
Dr. D. Copic, Prof. M. De Volder
Institute for Manufacturing
Department of Engineering
University of Cambridge
Cambridge CB3 0FS, UK
The ORCID identification number(s) for the author(s) of this article can be found under https://doi.org/10.1002/aelm.202001213.

DOI: 10.1002/aelm.202001213

back filled with Cu using a periodic pulsed reversed (PPR) electroplating process. Using this approach, we have been able to achieve SEC of $\sigma_p \approx 9.38 \times 10^4$ S cm^2 g^{-1} and ampacity of $A \approx 20 \times 10^5$ and 4×10^5 A cm^{-2} for 1.5 and 17 mm gauge length wires, respectively.

To produce CNTs/Cu composite using a CNTs filament, the most important challenge is to deposit Cu metal inside of the CNTs filament. Physical vapor deposition (PVD),[95–97] two-step galvanostatic electrodeposition,[98–100] and electrochemical deposition (DC electroplating) can potentially be used for depositing Cu on CNTs.[2,101,102] Among these, electroplating is a low cost, nonvacuum, and easily scalable metal deposition techniques. However, DC electroplating produces a Cu cladding on the CNTs filament surface that prevents the voids inside the CNTs matrix to be filled with copper and manifests as a (CNTs-core/Cu-shell) structure.[2,102] To overcome this problem, PPR electroplating[103–106] has been developed as a very effective technique for filling the voids/pores of the CNTs filament with Cu, obtaining a finer Cu grain size due to Cu dissolution during the reverse cycle and therefore enabling homogeneous Cu spatial distribution in the CNTs matrix.

In this work, we report the production of lightweight MWCNTs/Cu composite wires with homogeneously distributed Cu grains throughout an MWCNTs matrix. The key difference between our work from previous studies[2,95,97–102] is that the polymer surfactant which is used to disperse CNTs has been replaced with copper. Furthermore, due to the uniform dispersion achieved using microfluidization, removal of polymer surfactant creates an interconnected network of pores which allows the Cu to be penetrated deep into the filament during PPR electroplating as evidenced by field emission scanning electron microscope (FESEM) and energy-dispersive X-ray spectroscopy (EDS) analysis. To fabricate these composite wires, first MWCNTs filaments of diameter about 8 ± 0.3 µm are produced. Continuous MWCNTs filaments were spun by coagulation wet spinning in acetone and then to decompose the polymer the spun MWCNTs filaments were heated at 300 °C for 1 h. Subsequently, PPR electroplating, which includes a series of forward bias voltages followed by reverse voltages at a wide range of frequencies, was used for Cu electroplating. **Figure 1** presents a step-by-step schematic illustration of the fabrication process for creating MWCNTs/Cu composite wires which include MWCNTs dispersion, wet spinning, surfactant degradation, and PPR electroplating. Composite wires with average diameter of 10 ± 0.4 µm, specific weight of 5.9 ± 0.2 g cm^{-3}, tensile strength of 318 MPa, EC of $\sigma = 5.5 \times 10^5$ S cm^{-1} which corresponds to a specific electrical conductivity of 9.4×10^4 S cm^2 g^{-1}, and a maximum ampacity of $\approx 20 \times 10^5$ A cm^{-2} were achieved.

2. Results and Discussion

2.1. MWCNTs Dispersions

Due to the Van der Waals interactions, as received MWCNTs are bundled together and remain agglomerated after magnetic

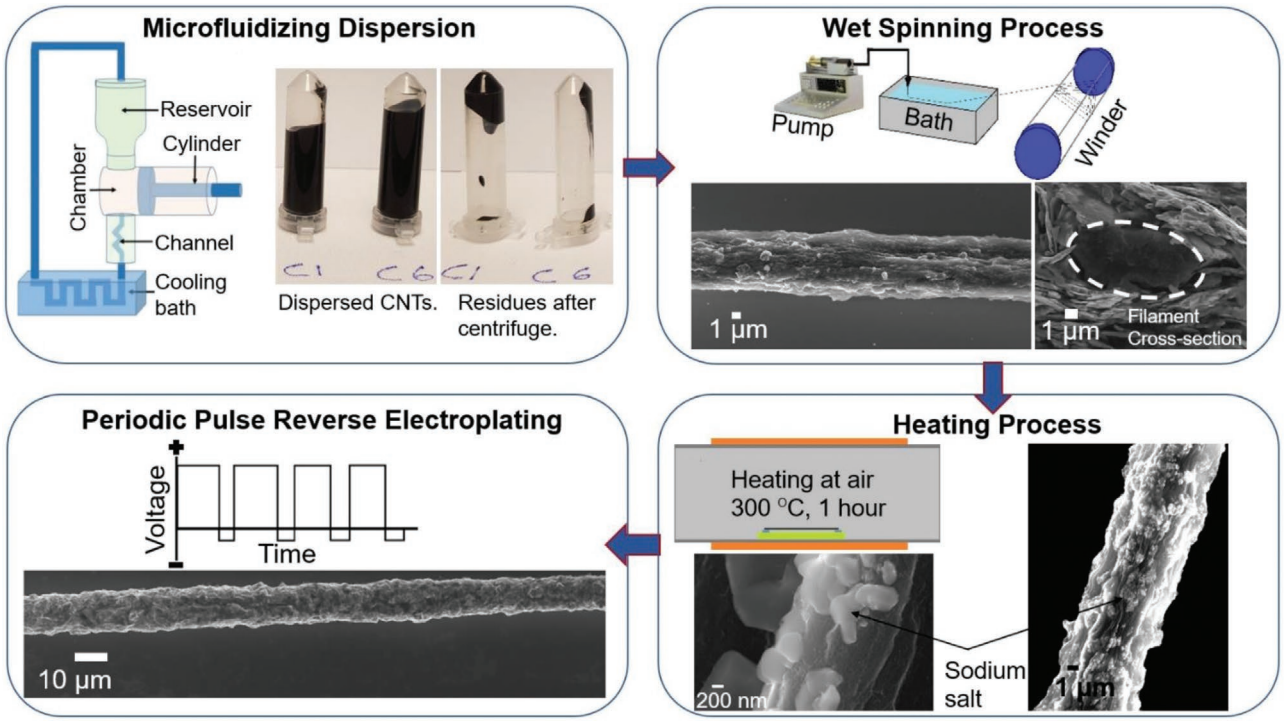

Figure 1. Step-by-step schematic of the fabrication protocol of the MWCNTs/Cu composite wires which includes: microfluidizer dispersion which comprises of LM20 microfluidizer schematic mechanism and comparison of the dispersed MWCNTs and residues after cycle 1 and 6 based on quantitative measurements of the weights of sedimentation, followed by the wet spinning process which comprises schematic of wet spinning, an SEM image of as-spun filament and its cross-section (Figures S1–S3, Supporting Information), followed by the heating process which shows SEM images of the heated filaments with sodium salt as bright cubic blocks distributed throughout the filament surface and followed by PPR electroplating process for the heated MWCNTs filaments and SEM image of MWCNTs/Cu composite wire.

stirring for 1 h, as shown in Figure S4a in the Supporting Information. To maximize their surface area and thus their properties, they need to be unbundled and dispersed uniformly. To achieve this, a very high MWCNTs concentration of 20 g L^{-1} with uniform dispersion is prepared using a scalable microfluidization process. MF is a system in which a large pressure of up to 30 000 psi (20.7×10^7 Pa), and a very high shear rate in the order of 10^6–10^8 s^{-1} are applied to the whole MWCNTs solution during the MF process.[107–110] Creating continuous MWCNTs filament is impossible without a very uniform MWCNTs dispersion. A comprehensive detail about the MF process for dispersing CNTs can be found in our recent work.[107] Even a small nonuniformity or agglomeration of MWCNTs can result in the breaking of the filament during wet spinning. MF has been used for dispersing as well as preparing the homogenous blending of MWCNTs in the polymer solution. Na-CMC has been used as a dispersant as well as a coagulating polymer.[111,112] Dispersion process details are discussed in the Experimental section. Figure S4 in the Supporting Information shows the SEM images of the MWCNTs before S4a and after S4b dispersion.

The most remarkable advantage of using MF is that all the CNTs present in the solution receive the same shear forces during dispersion, which is not possible to achieve using the conventional ultrasonication process.[109] To obtain a more quantitative measure for the dispersion quality, the sedimentation of the MWCNTs in the dispersion was measured after centrifuge. Centrifugal forces that enable the acceleration of the sedimentation of the dispersed CNTs bundles to the bottom of the cell, leading to a clarification of the dispersion were used.[110,113] Figure S4c in the Supporting Information compares the MWCNTs sediments after centrifuging at 10 000 rpm for 10 min. At 0 cycle, i.e., before the solution is passed through the MF, almost all the MWCNTs are sediments however after six cycles, sediments are about 2 wt% of the total solution. Furthermore, the MWCNTs water-based dispersion is produced at the rate of 0.6 L h^{-1} which is very fast as compared to the existing dispersion techniques like tip/bath sonication.[107–110]

2.2. Characterization of MWCNTs Filaments

Optimum values of surfactant-based coagulation spinning parameters (i.e., spinning solution injection rate, coagulation media, and take-up speed) which produced continuous flexible MWCNTs filaments were 1.8 mL h^{-1}, acetone, and 7 m min^{-1}, respectively. Filaments could not be spun continuously, from MWCNTs/Na-CMC solution, until the blending ratio was equal or greater than 1:4.6. As shown in the SEM micrographs of Figure 1, the MWCNTs/Na-CMC filaments exhibit a crimped, longitudinal grooved and intertwined surface texture and elliptical cross-section shape with a small filament diameter of 8 ± 0.3 µm. The formulation of this structure is due to counter diffusion of solvent/nonsolvent, phase separation during coagulation, and stretching force inside the coagulation bath.[114] Spun filaments were heated at 300 °C for 1 h to thermally decompose the Na-CMC polymer and the microstructure of the filaments became very porous, as shown in Figure 1 and Figure S4d in the Supporting Information. The bright cubic blocks distributed throughout the filament surface are believed to be the sodium salt which remains intact after thermal decomposition of CMC during the annealing process. However, the sodium salt crystals were completely dissolved during the MWCNTs filament incubation in the utilized aqueous electrolyte for about 20 s before the PPR electroplating which took about 360 s. SEM images in **Figure 2**a and Figure S4e,f in the Supporting Information show the MWCNTs/Na-CMC filament following annealing and aqueous electrolyte incubation which consist of loose fibrils and voids in the longitudinal and radial direction of filaments. During wet spinning, there is a draw ratio of ≈12.5 between the winding speed of 7 m min^{-1} and the extrusion speed at the spinneret of 0.56 m min^{-1}, which stretches the filament and partially aligns the CNTs as shown in Figure 2a.

2.3. Morphology and Structure of MWCNTs/Cu Composite Wires

To achieve the highest possible specific conductivity of MWCNTs/Cu wire and therefore the lowest Cu weight fraction, Cu nucleation, and growth rate were studied as a function of PPR electroplating parameters such as forward and reverse pulse voltage and electroplating current densities, reverse ratio and electrolyte concentration. PPR electroplating is advantageous over DC electroplating because it allows for the adjustment of key processing parameters that in turn enables nucleation and growth of fine and highly dense Cu grains.[103–106] In DC electroplating, deposition persists at the nucleation sites due to the continuous application of current, and thus grains with broader size distribution evolve.[104] PPR electroplating is optimized by varying voltage and current density to produce the smallest Cu grains and the maximum Cu penetration into the MWCNTs filament, as shown in Figure 2b. Grujicic and Pesic have shown that Cu electroplating on glassy carbon with lower deposition potential and lower current densities produce smaller Cu nuclei when compared to high current densities.[115] If the positive pulse voltage density (Cu deposition) is V_f with an on-time length of t_{fON} while the negative voltage density (Cu dissolution) is V_r with an on-time length of t_{rON}, the reverse ratio, δ, is defined as follows

$$\delta = \frac{V_r \times t_r}{V_f \times t_f} \times 100\% \quad (1)$$

The reverse ratio, δ, was varied from 0% to 62.5%. EC measurements of PPR electroplating at these reverse ratios δ, as shown in Figure S5 in the Supporting Information, indicated that EC decreases from $\sigma = 5.5 \times 10^5$ S cm^{-1} to $\sigma = 1.4 \times 10^5$ S cm^{-1} as the reverse ratio δ increases from $\delta = 0.62\%$ to $\delta = 62.5\%$. We believe that higher reverse ratio led to larger voids volume between Cu grains making the interconnection of Cu grains to be reduced and thus less EC values. Whereas a lower δ resulted in higher EC values due to smaller voids volume between Cu grains (highly dense and uniform deposit) and higher interconnection between Cu grains. PPR electroplating with a ratio δ of 0.625% has presented the lowest voids and thus highest interconnected Cu grains, the highest EC, the minimum outer coating thickness (or shell

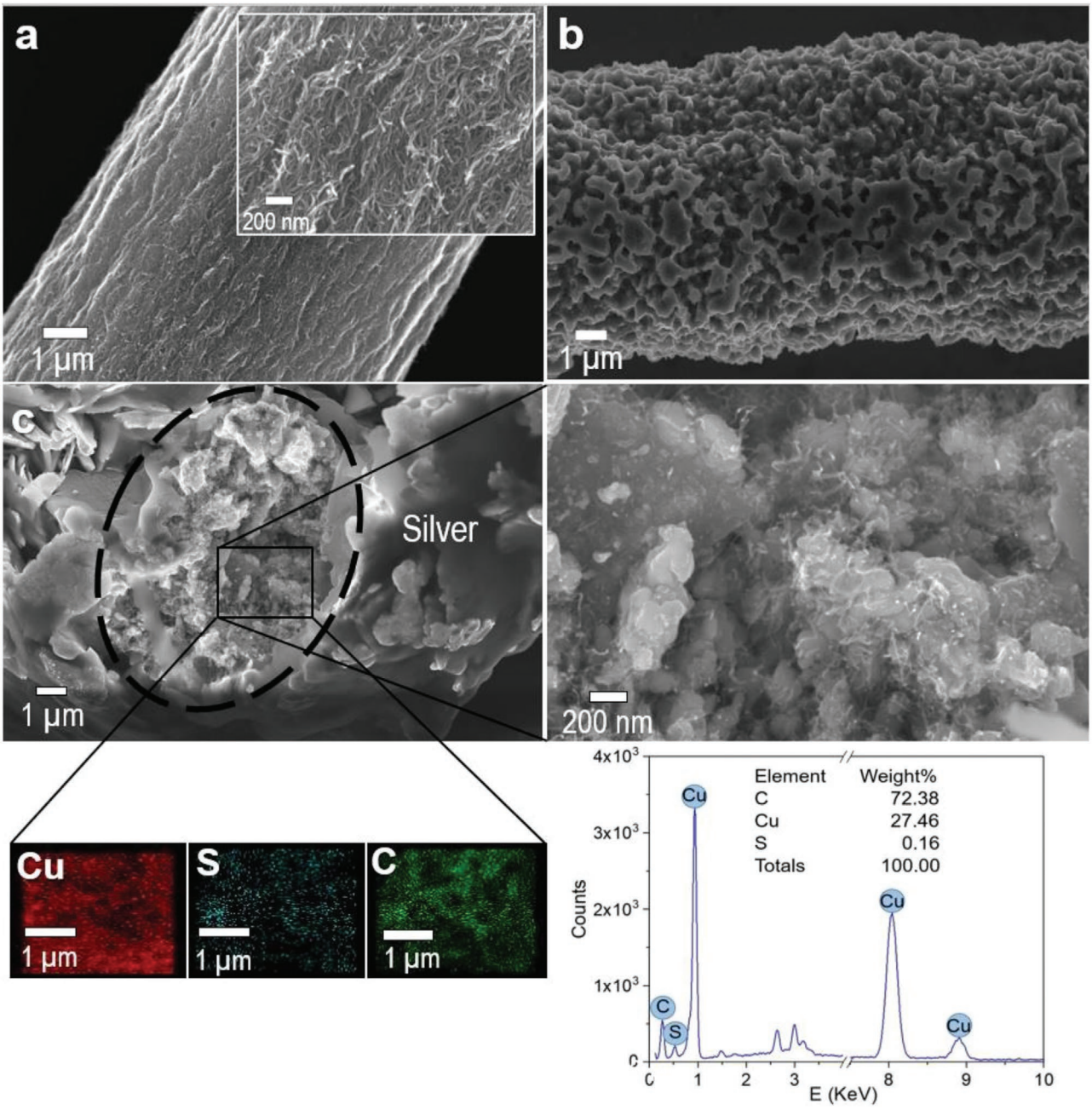

Figure 2. SEM images of a) MWCNTs/Na-CMC filament following annealing, aqueous electrolyte incubation, and drying, b) MWCNTs/Cu composite wire PPR electroplated with a ratio δ of 0.625%, c) cross-section of the MWCNTs/Cu wire indicated by a dashed line and the wires are surrounded by a silver glue which is used to hold the wire while cleaving the wire. EDS map of copper (Cu), sulfur (S), and carbon (C) and EDS spectrum of MWCNTs/Cu wire cross-section inside the box are cleared.

about 1 µm), and the highest ampacity. It is noteworthy that at $\delta = 0\%$, Cu only formed the outer coating of thickness about 2 µm.

Figure 2c shows a cross-section of an MWCNTs/Cu wire electroplated at a reverse ratio δ of 0.625% on an MWCNTs filament of diameter 8 ± 0.3 µm with mostly internal Cu filling and visible MWCNTs inside the Cu matrix. Cross-section of the wires was created after encapsulating the wires in the silver paste and then cleaving it.

In all the cross-section images, big particles around the wire are silver flakes. The diameter of the MWCNTs/Cu composite wire increased to 10 ± 0.4 µm after Cu PPR electroplating. The MWCNTs/Cu composite wire with mostly full Cu filling and interconnected Cu cladding shows a specific weight of 5.9 ± 0.2 g cm^{-3}, (2/3rd of Cu: 8.96 g cm^{-3}), indicating that MWCNTs has a volume fraction of 40%. To estimate the CNTs volume fraction, we have considered the density of MWCNTs to be 1.8 g cm^{-3}. Figure 2c shows the EDS map taken at the area indicated

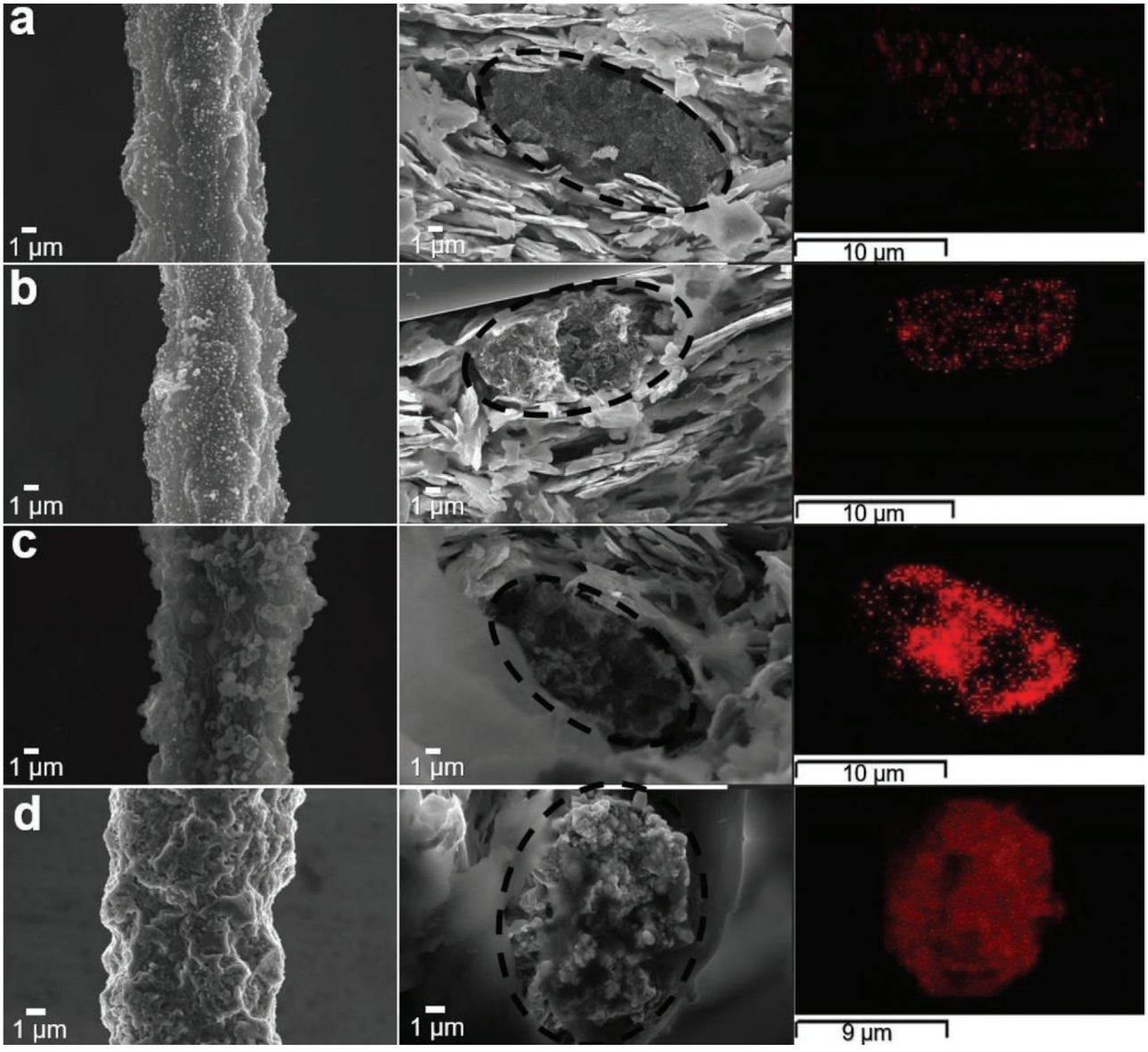

Figure 3. SEM images of the outer surface and its cross-section and Cu element distribution via EDS analysis of the MWCNTs/Cu wire PPR electroplated at a reverse ratio, δ of 0.625%, presenting the Cu nucleation rate/growth at different electrodeposition times a) 30 s, b) 90 s, c) 240 s, and d) 360 s.

by the black box, a strong copper signal confirms the penetration of Cu grains into the wire interior, filling the voids between individual MWCNTs and thus forming a structurally uniform MWCNTs/Cu composite wire. Furthermore, the EDS of sulfur element distribution shown in Figure 2c is due to the electrolyte infiltration along with the filament interfaces through the macromeso voids between MWCNTs bundles. It is worth noting that controlling the porous structure of the MWCNTs wet spun filaments through Na-CMC and MWCNTs weight ratio and the thermal decomposition of Na-CMC was indispensable to achieve structurally uniform MWCNTs/Cu distribution at high MWCNTs vol% in the composite wires.

Figure 3 shows a collage of images which include the outer surface of the wire, its cross-section and Cu element distribution measured via EDS analysis. These micrographs present the Cu nucleation growth as a function of electrodeposition times (30, 90, 240, and 360 s) at the reverse ratio, δ of 0.625%. To perform these measurements, four similar samples were used which have gone through the same electrodeposition process with the only difference that the electrodeposition was terminated at different times to capture the growth process. During the first 30 s of Cu deposition, 40–200 nm spheroidal small Cu seeds, sparsely populated, appeared both on the surface and inside of MWCNTs filament. Further PPR electroplating after 90 s causes additional seeding on the surface and into the MWCNTs filament with a larger size, 50–250 nm. The Cu seeds grew up and started merging and forming Cu grains, discontinuously distributed, in the interior and outer of the filament within 240 s. Finally, during 360 s of PPR electroplating, the Cu grains fully covered the 20 mm wire length and the voids and

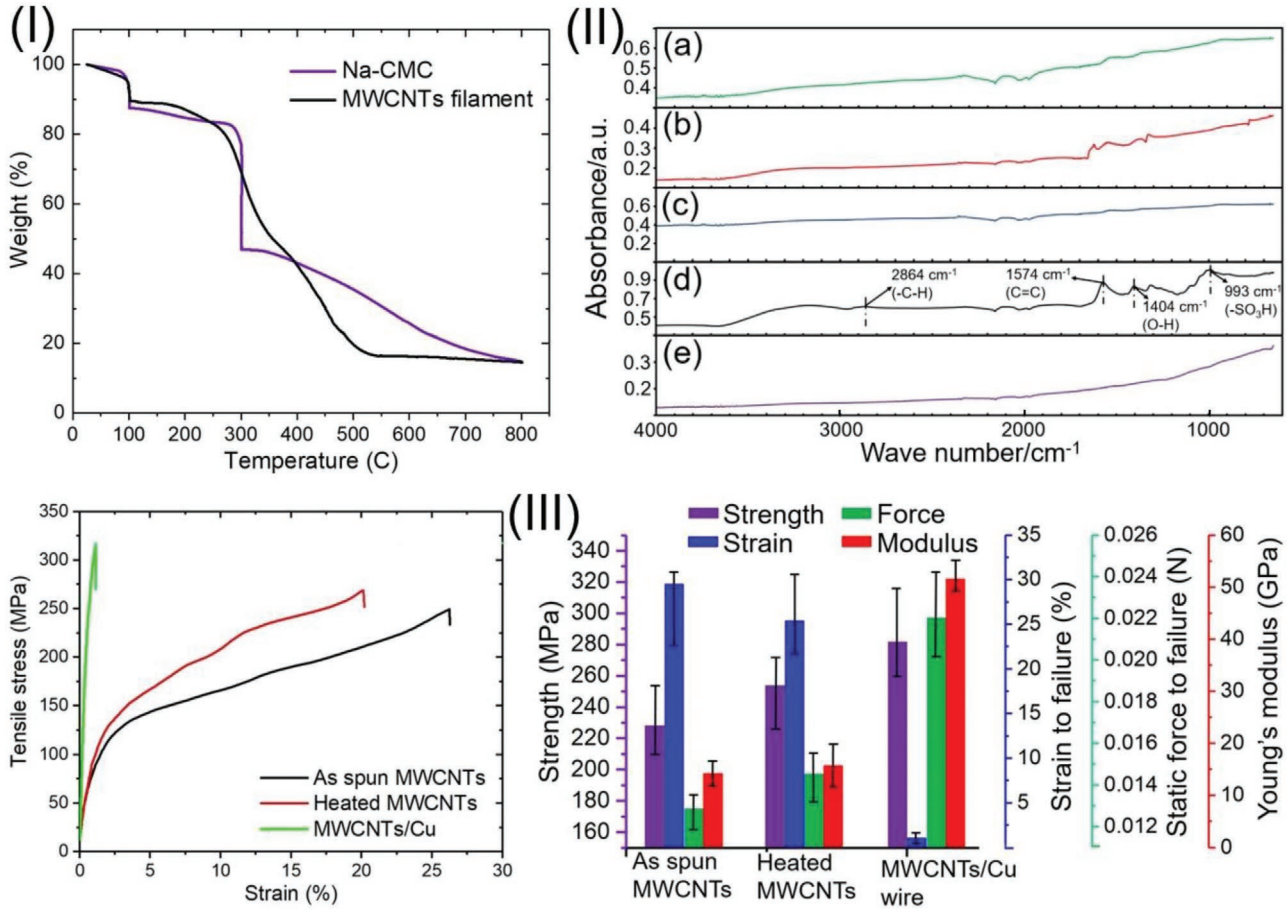

Figure 4. I) TGA curves of 1.6 wt% of Na-CMC film and as spun MWCNTs filament. II) FT-IR spectra of a) as spun, b) after heating at 300 °C for 1 h, c) following heating and incubation in DI water, d) following the PPR electroplating in aqueous electrolyte involved of sulfuric acid and DI water only without copper sulfate MWNTs filaments, and e) MWCNTs wire PPR electroplated with Cu. III) Tensile stress–strain curves and summarized mechanical properties of as-spun and heated MWCNTs filaments and MWCNTs/Cu wires.

spaces between MWCNTs bundles became mostly filled with Cu grains. MWCNTs/Cu composite wire was formed with compact and dense spheroidal/cubic Cu grains, 60–600 nm size, and continuously distributed and connected across the whole structure (Figures S6–S8, Supporting Information). To the best of the author's knowledge, there are no previous reports on the fabrication of CNTs/Cu composite wire with complete internal Cu grains filling in the wire cross-section by PPR electroplating.

2.4. Thermal Analyses of Na-CMC and MWCNTs Filaments

Figure 4I shows the thermogravimetric analyzer (TGA) thermograms of 1.6 wt% Na-CMC polymer and as spun MWCNTs filaments. Initial mass weight loss for Na-CMC polymer and MWCNTs filaments (about 7.1%) is considered due to the evaporation of the absorbed moisture trapped in the sample structure.[116] The mass weight loss due to thermal degradation of MWCNTs filament compounds was 25.92% at 300 °C based on the filament weight after subtracting the mass of evaporated water. However, this weight loss was high due to the 4.6 mass ratio of Na-CMC in the total mass of MWCNTs filaments. Whereas the mass weight loss of Na-CMC polymer was 49.96% at 300 °C during 1 h of heating. In other words, the TGA curve of Na-CMC distinctly indicates that nearly 50% of the mass weight was lost, elucidating the reason why MWCNTs filaments were heated at 300 °C for 1 h. The yield of the charred residue of MWCNTs filaments after thermal decomposition at 800 °C was 84.26%. Table S1 in the Supporting Information clarifies the mass weight loss of Na-CMC polymer and MWCNTs filaments as a function of heating temperature from 25 to 800 °C.

2.5. FT-IR Analysis of MWNTs Filaments and MWCNTs/Cu Composite Wires

Fourier transform infrared spectroscopy (FT-IR) spectra of MWNTs filaments and MWCNTs/Cu composite wires were recorded to identify changes in functional group composition during PPR electroplating. FT-IR was performed on a collection/wool of hundreds of filaments. Figure 4IIa–c presents the FT-IR of three samples a) as-spun filaments, b) after heating at 300 °C and 1 h, and c) after soaking the heated filaments in deionized (DI) water for 15 min. It has been noticed the absence of any significant peaks in the as-spun filaments or heated filaments due to the fabrication of MWCNTs without

any functional groups. FT-IR spectrum of MWNTs filaments following the PPR electroplating in Figure 4IId, with aqueous electrolyte involved of sulfuric acid and DI water only without copper sulfate, introduced two oxygen-containing functional groups at the MWCNTs surface. These groups perform as active Cu deposition sites for as long as Cu electrodeposition is the interaction of applied voltage and the reduction of functional groups.[103,117] The presence of a peak at 993 cm^{-1} which is corresponding to –SO3H indicates the formation of sulfonic functional groups on the sidewalls of the carbon nanotubes.[118,119] The peak at 1404 cm^{-1} is assigned to the bending vibration of O–H in aliphatic hydroxyl bending due to the partial oxidation of MWCNTs in the sulfonation process.[120] The peak at 1574 cm^{-1} is attributed to C=C graphitic stretching of MWCNTs backbone, due to activation in the reverse electroplating process.[119] Finally, the peak at 2864 cm^{-1} is assigned to asymmetric and symmetric stretching vibration band of methylene —C—H located at defect sites on benzene rings of nanotubes.[120,121] FT-IR spectrum of an MWCNTs wire PPR electroplated with Cu (Figure 4IIe) confirmed the interface between the Cu and MWCNTs as the indicated peaks became smaller and nearly disappeared.[102]

2.6. Mechanical Properties of MWNTs Filaments and MWCNTs/Cu Composite Wires

Figure 4III compares the mechanical properties of as-spun and heated MWCNTs filaments and MWCNTs/Cu wires. The tensile stress–strain curves of these filaments and wires show analogous behavior, which includes three stages: elastic deformation, plastic deformation, and fracture stage. Corresponding average values of the tensile strength (MPa), strain to failure (%), static force to failure (N), and Young's modulus (GPa) were calculated using the linear, plastic and failure stages of the stress–strain curves and are reported in Figure 4III. Other than the as-spun state, the introduction of heating at 300 °C for 1 h led to very slightly improved tensile strength, static force to failure and Young's modulus but a reduced strain to failure, which is due to an increased sliding resistance and reduced contact resistance between the MWCNTs bundles.[95] It is clear from the stress–strain curves that Cu PPR electroplating with high internal Cu filling induced interfacial adhesion, friction, and good contact between the Cu and MWCNTs. Eliminating the pores and gaps and suppressing the slippage between the MWCNTs bundles, enabled increased load-bearing capability. As a result, the tensile strength of the MWCNTs/Cu composite wires reached 318 MPa (by comparison with pure Cu which has a tensile strength of 200 MPa for coarse-grained Cu and tensile strength of 270 MPa for initial pure Cu[122]), a 117% and 127% increase than those of the heated and as spun MWCNTs filaments, respectively.

In addition, the elastic Young's modulus of the MWCNTs/Cu composite wires attained a 53.78 GPa which is 356% and 360% higher than those of the heated and as spun MWCNTs filaments, respectively. Whereas the strain to failure of the MWCNTs/Cu composite wires diminished to 1.8%, 6.92%, and 6.27% lower than those of the heated and as spun MWCNTs filaments, respectively. These measurements show that Cu PPR electroplating has enhanced the tensile strength and Young's modulus of the MWCNTs filament rather than weakened it. SEM analysis of MWCNTs/Cu wire fracture surface at tensile failure manifests both local necking and pull-out of the MWCNTs as shown in Figure S9 in the Supporting Information.

2.7. EC of MWCNTs/Cu Composite Wires

The EC of the MWCNTs/Cu composite wire is substantially increased after Cu electroplating. Before Cu PPR electroplating, the heated MWCNTs filaments had an average EC of $\sigma = 65$ S cm^{-1}, which was tenfold higher than the as-spun filaments, which have an average EC of $\sigma = 6.4$ S cm^{-1}. After Cu PPR electroplating, the EC of MWCNTs/Cu wires increased up to $\sigma = 5.5 \times 10^5$ S cm^{-1} which corresponds to an SEC of 9.4×10^4 S cm^2 g^{-1}, it is 45% higher than the 100% international annealed copper standard (IACS) Cu specific electrical conductivity of $\approx 6.5 \times 10^4$ S cm^2 g^{-1}. Since 2010, there has been significant progress in improving the electrical conductivity of macroscopic CNTs/metal composite wires.[2,95,97–102,123] **Figure 5**a presents Ashby plots of EC versus CNTs/metal composite wires specific weight such as CNTs/Au, CNTs/Pt, CNTs/Pd,[101] CNTs/Ag,[123] and CNTs/Cu.[2,95,97–102] Cu based CNTs composites have higher EC as compared to Au, Pt, Pd, and Ag composites. Their corresponding specific electrical conductivities are presented in Figure S10 in the Supporting Information. In CNTs/metal composites, an optimum amount of CNTs are required to achieve maximum SEC. As the volume fraction of CNTs approaches zero, CNTs/Cu composite has similar conductivity and density as the metal. For example, ref. [2], which uses only 2 vol% of CNTs and has an EC $\sigma = 5.68 \times 10^5$ S cm^{-1}. Recently there have been a few studies where CNTs filaments have been coated with Cu shell and by optimizing the thickness of the Cu layer, SEC has been optimized. Reference [95] reported an SEC about 35% more than copper but their measurements were based on the density of CNTs core wire to be 1 g cm^{-3}, however, the electrical conductivity of the core was not reported. In this work we have fabricated MWCNTs/Cu composite wires where copper grains mostly fill the CNTs matrix. About 40 vol % of individual MWCNTs are spatially distributed uniformly throughout the structure with specific weight 2/3rd of Cu. We have measured the electrical conductivity of twenty MWCNTs/Cu composite wires, which varied from 4.5×10^5–5.5×10^5 S cm^{-1}. Highest EC was 5.5×10^5 S cm^{-1} and corresponding SEC was $\sigma_\rho \approx 9.4 \times 10^4$ S cm^2 g^{-1} which is 45% higher than 100% IACS Cu. The mean and median EC values are 5.1×10^5 and 5.2×10^5 S cm^{-1}, respectively, standard deviation (SD) is 0.36×10^5 S cm^{-1}. Using 20 measurements, mean and median SEC are 8.6×10^4 and 8.8×10^4 S cm^2 g^{-1}, respectively, SD is 6.1×10^3 S cm^2 g^{-1} and the minimum and maximum measured values are 7.7×10^4 S cm^2 g^{-1} and 9.4×10^4 S cm^2 g^{-1}, respectively. We believe that the excellent EC in this work is attributed to the small Cu grain distributed uniformly in the MWCNTs matrix which is attached with moderately functionalized MWCNTs and promote an efficient electron transfer between Cu and CNTs and form a highly interconnected Cu and CNTs network.[124,125]

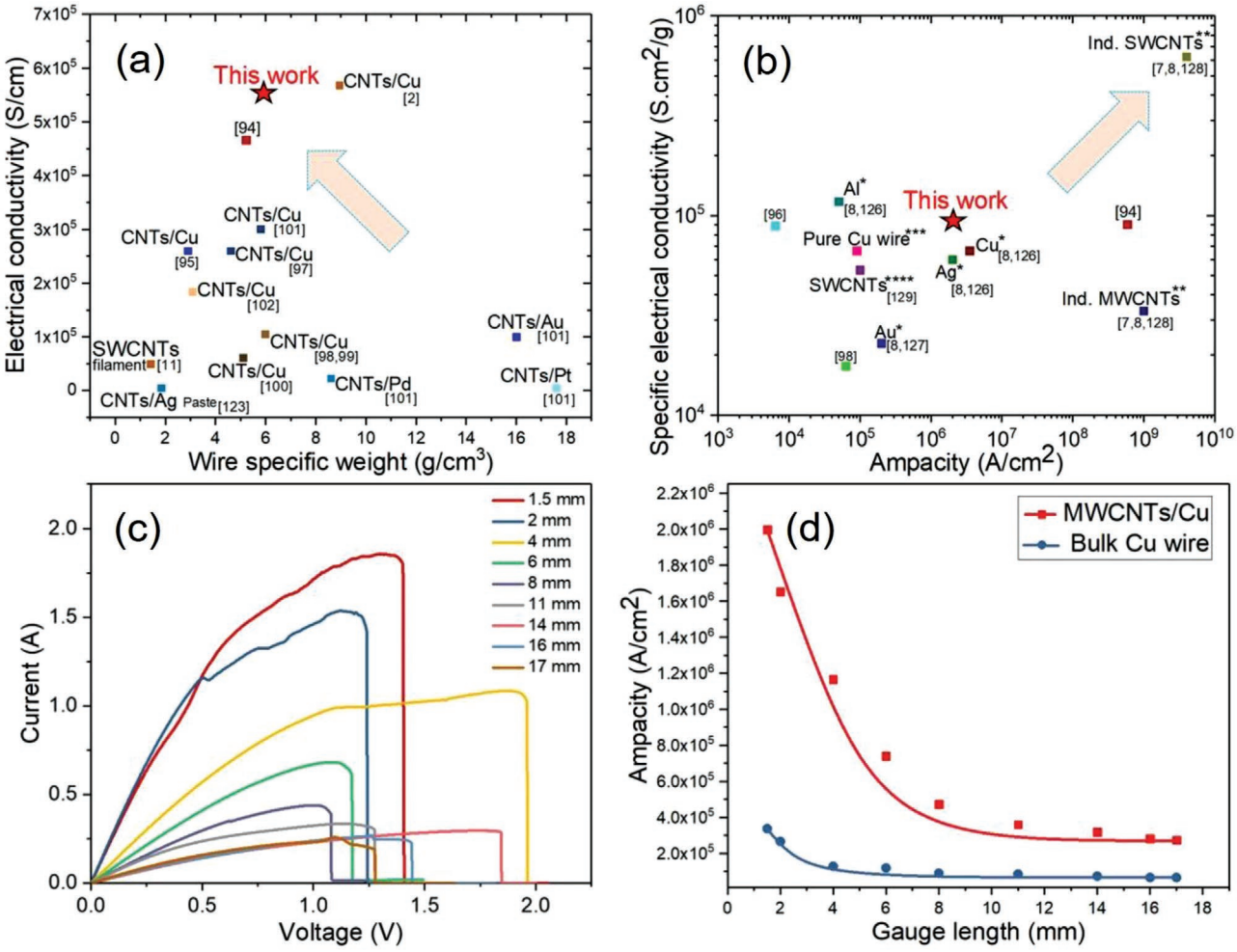

Figure 5. a) Ashby plots of electrical conductivity versus wire specific weight for MWCNTs/Au, Pt, Pd, Ag, and Cu composite wires. Pure SWCNTs filaments were also presented for comparison with this work performance of MWCNTs/Cu composite wire exceeding it. b) Ashby plots of specific electrical conductivity (SEC) versus ampacity for published CNTs/Cu composite wires. As shown, this work MWCNTs composite wire is overrunning a unique position with high ampacity and SEC. (*) polycrystalline Cu, Au, Ag, and Al metals, (**) individual multi and single-wall carbon nanotubes, (***) our measurements on pure Cu wires, and (****) super-acid spun SWCNTs filaments (DEXMAT CO., www.dexmat.com)[129]. c) *I–V* curves of MWCNTs/Cu composite wire electroplated with different ampacity gauge length measurements. d) Differentiation curves of ampacity values for MWCNTs/Cu composite wires and pure Cu wire at different gauge lengths.

2.8. Ampacity of MWCNTs/Cu Wires

Here, ampacity is defined as the maximum current density which flows through the wire before it becomes an open circuit. It is measured using the formula

$$\mathrm{Amp}_{\max} = \frac{I_{\max}}{A_{\mathrm{CS}}} \tag{2}$$

where $I_{\max}$ is the maximum current before failure and A_{cs} is the cross-section area of the wire. Figure 5b presents SEC versus ampacity which compares our results with other published work on CNTs/Cu wires,[96,98] polycrystalline metals such as Cu, Au, Ag, and Al,[8,126,127] individual multi and single-walled carbon nanotubes[7,8,128] and our measurements of commercially available super-acid spun CNTs filaments DEXMAT CO., and pure Cu wires (ϕ 0.05 mm, the scientific wire co. Essex, UK).

Electrical conductivity and the specific electrical conductivities reported in this paper are also very similar to the values reported by Subramanian et al.,[94] which demonstrate very similar material properties. However, there are two main differences. First, we have fabricated and performed measurements on free-standing MWCNTs/Cu wires which has a potential for scaling up, whereas wires reported in ref. [94] are lithographically defined. Second, their CNTs are grown and fabricated on a same substrate, which provides a good thermal contact with the silicon substrate, leading to a very good thermal dissipation hence very high ampacity. In case of free-standing wires, they only have a good thermal contact at the end of the wires where these are attached with silver contact pads. Therefore, ampacity of free-standing wires is very low in comparison with ref. [94] and ampacity of our wires increases as the length of the MWCNTs/Cu wire is decreased.

Figure 5c presents *I–V* curves of MWCNTs/Cu composite wires, PPR electroplated at a reverse ratio δ of 0.625% and measured at different gauge lengths (1.5–17 mm). Initially the current increases linearly as the voltage are increased and at this stage the measured electrical resistivity is almost constant, and the MWCNTs/Cu composite wires with shorter length have a higher slope due to their smaller resistance. As these wires heat up due to Joule heating, their resistance is increased, and IV curves enter the nonlinear regime and eventually become an open circuit. These curves provide the maximum current value (I_{max}) of the MWCNTs/Cu composite wires at different lengths form which the maximum current density or ampacity is calculated. For example, the I_{max} value of 1.857 A for 1.5 mm wire length and 93 μm^2 cross-section areas gave ampacity of 19.97×10^5 A cm^{-2} and for the I_{max} value of 0.259 A for 17 mm wire length and cross-section of 93 μm^2 ampacity was 2.74×10^5 A cm^{-2}. Presence of CNTs in CNTs/Cu composite wires inhibits the surface and grain boundary Cu diffusion due to interlocking friction[8,94] and increase Cu diffusion activation energy (≈2.0 eV vs 0.6–1.0 eV in pure Cu),[94,130] which suppress Cu electromigration in the Cu/CNTs composite and therefore increase its ampacity.

Figure 5d compares the ampacity values for MWCNTs/Cu composite wires and pure Cu wire at different gauge lengths. The ampacities for both MWCNTs/Cu wire and Cu increase as the length of the wire is decreased due to the existence of more nanometer-scale voids or other defects at longer wire length. When a high current density flows through the wires, the center of the wire has the highest temperature due to Joule heating. As the length of the wire is decreased, heat can more easily be dissipated through the contact pads which behave like heat sinks. These measurements show that for longer wires, where ampacity is independent on length, Joule heating is a dominant mechanism that determines the ampacity of the wires. Whereas for smaller wire lengths, electromigration plays a dominant role in determining the ampacity of the wire.[124,125] The difference between the Cu/CNTs composite wire and the Cu wire is likely due to the higher thermal conductivity of the Cu/CNTs[131] and the increased Cu diffusion activation energy in Cu/CNTs composite.[130,131] High thermal conductivity of CNTs which dissipate Joule heating more efficiently than Cu may lead to a sharp increase in the ampacity of CNTs/Cu than Cu for shorter gauge lengths. Magnified images of MWCNTs/Cu wire mechanical failure mode following the ampacity test indicate the presence of MWCNTs in the destructive points with Cu grains detection, as shown in Figure S11 in the Supporting Information.

3. Conclusion

In this work, we have reported a simple acid free wet spinning method for creating continuous MWCNTs filaments with a diameter 8 ± 0.3 μm. To make continuous filaments, a very high concentration (20 g L^{-1}) and a very uniform dispersion of MWCNTs are formulated using a water-based microfluidization process which is a very scalable and high throughput method. MWCNTs/Cu composite wires are then produced using PPR electroplating of MWCNTs filaments using various reverse ratios δ, 0–62.5%. The reverse ratio δ of 0.625 has resulted in the lowest Cu volume fractions, and the highest EC and ampacity. These MWCNTs/Cu wires are 2/3rd the weight of bulk Cu wires. Their specific electrical conductivity is $\sigma_\rho \approx 9.4 \times 10^4$ S cm^2 g^{-1} which is 45% higher than IACS Cu, and the ampacity is four to six times higher than bulk Cu wires. These MWCNTs/Cu composite wires are very promising as lightweight and high-power transmission wiring in the current and next-generation electrical and electronic devices and systems.

4. Experimental Section

Materials: MWCNTs were purchased from US Research Nanomaterials, Inc. (Houston, USA). According to the supplier datasheet, these MWCNTs have a purity > 95 wt%, surface area: 500 m^2 g^{-1} brunauer–emmett teller, electrical conductivity >100 S cm^{-1} and impurities are 0.19% aluminum, 0.58% chlorine, 1.01% cobalt, 0.24% sulfur, 0.33% manganese, and 0.18% oxygen. Carbon is 97%, (Figure S12, Supporting Information). Na-CMC of MW 700 000 g mol^{-1} was purchased from Sigma-Aldrich (Gillingham, UK).

Dispersion and Spinning Dope Solution Preparation: MWCNTs in DI water at a (C = 20 g L^{-1}) with Na-CMC at a (C = 3 g L^{-1}) were magnetically stirred for 24 h and de-agglomerated and dispersed by a microfluidizer (MF) (LM20, MicrofluidicsTM, Newton, USA), with a Z type H210Z single microchannel, which has a hydraulic diameter of 200 μm. 100 mL batch was processed at 5000 PSI, six processing cycles at the rate of 1 mL per cycle s^{-1}. Subsequently, dispersed MWCNTs were mixed at a 1:4.6 ratio with an aqueous solution of 1.6 wt% of Na-CMC by MF with four cycles at 5000 PSI and another four cycles at 2000 PSI. To quantitatively characterize the MWCNTs dispersion, the sedimentation was evaluated using a centrifuge 5418R (Eppendorf UK Limited, Stevenage, UK). 0.2 mL was inserted in the measurement cells and centrifuged at 10 000 rpm for 10 min at room temperature. The weights of sedimentation were measured to determine the efficiency of dispersion.

Surfactant-Based Coagulation Wet Spinning: The dispersed solution of MWCNTs/Na-CMC was fed from a 20 mL capacity syringe (Fisher Co., Leicestershire, UK) to a vertically orientated (25 gauge) flat-ended metal needle "spinneret" via Teflon tubing. The inner and outer diameters of the needle were 0.26 and 0.515 mm, respectively. The volume feed rate was digitally controlled by a positive displacement microprocessor syringe pump (KD Scientific Inc., Holliston, MA, USA). A spinning solution feed rate of 1.8 mL h^{-1} was maintained and acetone was used as a coagulant bath at room temperature. Hundreds of meters long filaments were collected on a three wires take-up winder outside the bath at a rate of 7 m min^{-1}. Figures S1–S3 in the Supporting Information of MWCNTs filaments spun continuously and collected on a winder. Filaments were dried at room temperature for 24 h to remove any residual solvents. Then, filaments were heated in a compact horizontal tube furnace (Carbolite Gero Co. Hope, UK) at 300 °C for 1 h to decompose the Na-CMC polymer.

Periodic Pulse Reverse (PPR) Electroplating of Cu into MWCNTs Filaments: MWCNTs filament (diameter of ≈8 ± 0.3 μm and length of 20 mm) as a cathode and Cu electrode (60, 10, and 0.65 mm) as an anode were immersed in a glass cell with a volume of 0.05 dm^3 and the aqueous electrolyte utilized involved of 32 mL copper sulfate pentahydrate (1 mole), 4 mL sulfuric acid (5 moles), and 4 mL DI water. The experimental setup is illustrated in Figure S13a in the Supporting Information. The upper end of MWCNTs filament was mounted on a silicon wafer substrate by a silver paint outside the electrolyte bath to make electrical contact via a copper wire and the lower end of MWCNTs filament was mounted on the substrate inside the electrolyte bath by photoresist as a nonconducting glue. Silver paint and glue were dried overnight at room temperature. PPR electroplating was performed by using potentiostat/galvanostat electrochemical station

controlled by EC-Lab software (SP200, BioLogic Science Instruments, Grenoble, France) and applying periodic pulsed voltage cycles between the MWCNTs filament and Cu electrode as shown in Figure S13b in the Supporting Information. During PPR electroplating, deposition and the removal of Cu happen alternatively on every pulse, depending on the polarity of the pulses. The current density was in the rage of 10–50 mA cm^{-2}. To calculate the current density, the geometrical surface area of the filament was used without accounting for the porosity. Also, the forward pulse voltage density, V_f, was (40–120) V cm^{-2} and ON time, t_{fON}, was 80 ms. The reverse pulse voltage density, V_r, was 6–240 V cm^{-2} and ON time, t_{rON}, was (10–25) ms, repeated for 4000 cycles.

Morphological, Thermal, Chemical, Mechanical, and Electrical Characterization: Surface morphology and the diameter of the filaments and composite wires and Cu nuclei were observed by FESEM (Leo 1530 VP, New York, USA), with an acceleration voltage of 15 kV and Gallium focused ion beam (Zeiss Orion NanoFab GaFIB, Germany). Cu nuclei analysis and elemental quantitative mapping were analyzed by EDS with INCA mapping and analyzer software (Oxford Instruments Nanoanalysis, High Wycombe, UK). The internal structure and Cu spatial distribution in the various types of MWCNTs/Cu wires were obtained by characterizing multiple cross-sections in FESEM attached with an EDS. To estimate the uniformity of the MWCNTs/Cu wires, the diameter was measured at least in ten points along the length of a 20 mm long MWCNTs/Cu wire. A mean diameter of the wires was 10 μm and the standard deviation was 0.24 μm, which shows that the wire diameter does not vary more than 5% over the length of a wire. To measure the electrical conductivity of the MWCNTs/Cu wires, the cross-section images of 12 wires were taken using an FESEM. These images are shown in Figure S14 in the Supporting Information. A mean cross-section area is 86 μm^2 and the SD is 6.8 μm^2 and the maximum area is 93 μm^2. Since the conductivity is inversely proportional to the cross-section area, to avoid any over estimation of conductivity, the maximum area value was used to calculate the electrical conductivity of all the MWCNTs/Cu wires. Table S2 in the Supporting Information shows the resistance of 20 devices which were analyzed, and their lengths vary from 1.5 to 17 mm. These resistance values are provided without correcting the total contact resistance, which was negligible, ≈0.05 Ω from both contacts. Contact resistance was measured using a transmission line and after plotting resistance as a function of length. Having used the maximum area of 93 μm^2, EC and SEC of these 20 devices are given in the last two columns. To study the filament/wire cross-section, first the filament/wire was placed on the surface of a silicon chip of area about 1 cm × 1 cm and covered the filament/wire with the silver paste. Once the silver paste is completely dried, the silicon wafer was partially scribed with a diamond scriber and then cleaved along the scribed line. These cleaved samples were then vertically mounted on an SEM stub for taking SEM images and EDS analyses. For all the cross-section images, filaments/wires are surrounded by silver flakes, which come from the silver paste. Silver is used because in EDS spectrum its signal is clearly distinguished from copper. The cross-section areas of the filaments/wires obtained from SEM images were calculated via Image J software (cross-section area was assumed as elliptical) as shown in Figure S14 in the Supporting Information. The volumetric density of the MWCNTs/Cu wire is measured by calculating the volume of the wire which is the area of 93 μm^2 times the length of the wire and the weight is measured using a high precision Sartorius ultramicro balance which had a resolution of 0.1 μg (Sartorius, Germany). Thermal analyses of Na-CMC polymer and as spun MWCNTs filaments which include mass weight loss wt% as a function of heating temperature were conducted to determine the amount of Na-CMC in the MWCNTs filaments by using a TGA (Pyris1 TGA, PerkinElmer, Llantrisant, UK). A heating temperature of 25–800 °C and a heating rate of 10 °C min^{-1} in the air with a flow rate of 20 mL min^{-1} were applied. To evaporate any residual solvent and moisture, both specimens were held for 15 min at 100 °C and to understand the polymer decomposition, Na-CMC polymer (film) was also held for 1 h at 300 °C. Filament/wire chemical information was acquired via an FT-IR Spectrometer (Frontier, PerkinElmer, Massachusetts, USA). Scans were taken in the range of 4000–650 cm^{-1} and 64 repetitions were averaged for each spectrum. The resolution was 4 cm^{-1} and the scanning interval was 2 cm^{-1}. Mechanical properties (Young's modulus, strain to failure, static force to failure, and tensile strength) of MWCNTs filaments and MWCNTs/Cu wires were tested in dry condition by using dynamic mechanical analysis Q800 Dynamic mechanical analysis (TA Instruments, New Castle, USA) with a 0.00001 N force resolution. Tensile tests were carried out at a temperature of 25 °C and relative humidity of 65% with a force ramp rate of 0.005 N min^{-1} and a gauge length of 5 mm. For each kind of filament/wire, at least three tests were repeated. EC values were obtained at room-temperature by four-point probe resistance measurements using Keithley 5200 SCS parameter analyzer (Keithley A Tektronix company, Bracknell, UK). EC[S cm^{-1}] is defined as follows

$$EC = \frac{L}{R.A} \times 10^{-2} \tag{3}$$

where L is the wire length[m], R is the wire electrical resistivity[Ω], and A is the wire cross-section area [m^2]. Conducting silver paint was used to make electrical pads and the silver paint was dried overnight at room temperature. The ampacity of the MWCNTs/Cu wires was measured at a laboratory atmosphere using Keithley 2651A high power system source meter SMU instruments (Keithley A Tektronix company, Bracknell, UK). Here, the ampacity of the wire is defined as the maximum current density which flows through the wire before it becomes an open circuit.

The volume fraction of CNTs in the Cu/CNTs composite wires was calculated using the formula

$$\rho_{wire} = \rho_{Cu}\left(\frac{R}{1+R}\right) + \rho_{CNTs}\left(\frac{1}{1+R}\right) \tag{4}$$

where ρ_{wire} = 5.9 g cm^{-3}, ρ_{Cu} = 8.96 g cm^{-3}, and ρ_{CNTs} = 1.8 g cm^{-3} are the densities of the composite wires, copper, and CNTs, respectively, and $R = V_{Cu}/V_{CNTs}$ is the ratio of the copper and CNTs volumes. It is estimated that more than 75% of the pores are refilled with copper as discussed in estimation of the percentage of pores filled with copper paragraph and Figure S15 in the Supporting Information. In addition, the percolation analysis was included in Figure S16 in the Supporting Information.

Supporting Information

Supporting Information is available from the Wiley Online Library or from the author.

Acknowledgements

M.B.B. and A.A. contributed equally to this work. All the authors acknowledge the support of the Lloyd's Register Foundation (LRF), London, UK, which funded this research through their grants to protect life and property by supporting engineering-related education, public engagement, and the application of research (Grant Reference: LloydsRegisterFdn-G0083). The authors are also grateful to Dr. Changshin Jo for performing TGA and Dr. Giorgio Divitini for performing transmission electron microscopy measurements.

Conflict of Interest

The authors declare no conflict of interest.

Data Availability Statement

The data that support the findings of this study are openly available.

Keywords

ampacity, carbon nanotubes, composite wires, copper, microfluidization

Received: December 10, 2020
Revised: January 24, 2021
Published online: March 12, 2021

[1] S. Zhang, N. Nguyen, B. Leonhardt, C. Jolowsky, A. Hao, J. G. Park, R. Liang, *Adv. Electron. Mater.* **2019**, *5*, 1800811.
[2] P. M. Hannula, A. Peltonen, J. Aromaa, D. Janas, M. Lundstrom, B. P. Wilson, K. Koziol, O. Forsen, *Carbon* **2016**, *107*, 281.
[3] R. H. R. Castro, P. Hidalgo, E. C. Diniz, *Mater. Lett.* **2011**, *65*, 271.
[4] F. A.-D. S. Rodrigues, W. Paraguassu, S. Simoes, M. F. G. Vieira, J. A. D.-S. Souza, E. D.-M. Braga, M. A. L.-D. Reis, *J. Nanosci. Nanotechnol.* **2017**, *17*, 4837.
[5] M. F. L. De Volder, S. H. Tawfick, R. H. Baughman, A. J. Hart, *Science* **2013**, *339*, 535.
[6] R. Rao, C. L. Pint, A. E. Islam, R. S. Weatherup, S. Hofmann, E. R. Meshot, F. Wu, C. Zhou, N. Dee, P. B. Amama, J. Carpena-Nunnez, W. Shi, D. L. Plata, E. S. Penev, B. I. Yakobson, P. B. Balbuena, C. Bichara, D. N. Futaba, S. Noda, H. Shin, K. S. Kim, B. Simard, F. Mirri, M. Pasquali, F. Fornasiero, E. I. Kauppinen, M. Arnold, B. A. Cola, P. Nikolaev, S. Arepalli, H.-M. Cheng, D. N. Zakharov, E. A. Stach, J. Zhang, F. Wei, M. Terrones, D. B. Geohegan, B. Maruyama, S. Maruyama, Y. Li, W. W. Adams, A. J. Hart, *ACS Nano* **2018**, *12*, 11756.
[7] A. Chinnappan, C. Baskar, H. Kim, S. Ramakrishna, *J. Mater. Chem. A* **2016**, *4*, 9347.
[8] R. M. Sundaram, A. Sekiguchi, M. Sekiya, T. Yamada, K. Hata, *Royal Soc. Open Sci.* **2018**, *5*, 180814.
[9] P. Dariyal, A. K. Arya, B. P. Singh, S. R. Dhakate, *J. Mater. Sci.* **2021**, *56*, 1087.
[10] R. J. Headrick, D. E. Tsentalovich, J. Berdegue, E. A. Bengio, L. Liberman, O. Kleinerman, M. S. Lucas, Y. Talmon, M. Pasquali, *Adv. Mater.* **2018**, *30*, 1704482.
[11] N. Behabtu, C. C. Young, D. E. Tsentalovich, O. Kleinerman, X. Wang, A. W. K. Ma, A. A. Bengio, R. F. Waarbeek, J. J. de-Jong, R. E. Hoogerwerf, S. B. Fairchild, J. B. Ferguson, B. Maruyama, J. Kono, Y. Talmon, Y. Cohen, M. J. Otto, M. Pasquali, *Science* **2013**, *339*, 182.
[12] V. A. Davis, N. G. Parra-Vasquez, M. J. Green, P. K. Rai, N. Behabtu, V. Prieto, R. D. Booker, J. Schmidt, E. Kesselman, W. Zhou, H. Fan, W. W. Adams, R. H. Hauge, J. E. Fischer, Y. Cohen, Y. Talmon, R. E. Smalley, M. Pasqual, *Nat. Nanotechnol.* **2009**, *4*, 830.
[13] L. M. Ericson, H. Fan, H. Peng, V. A. Davis, W. Zhou, J. Sulpizio, Y. Wang, R. Booker, J. Vavro, C. Guthy, A. N. G. Parra-Vasquez, M. J. Kim, S. Ramesh, R. K. Saini, C. Kittrell, G. Lavin, H. Schmidt, W. W. Adams, W. E. Billups, M. Pasquali, W.-F. Hwang, R. H. Hauge, J. E. Fischer, R. E. Smalley, *Science* **2004**, *305*, 1447.
[14] W. J. Lee, A. J. Clancy, J. C. F. Toribio, D. B. Anthony, E. R. White, E. Solano, H. S. Leese, J. J. Vilatela, M. S. P. Shaffer, *Carbon* **2019**, *146*, 162.
[15] H. Mirbaha, P. Nourpanah, P. Scardi, M. Dincau, G. Greco, L. Valentini, S. B. Bon, S. Arbab, N. Pugno, *Materials* **2019**, *12*, 2797.
[16] J. Y. Kim, J.-H. Mo, Y. H. Kang, S. Y. Cho, K.-S. Jang, *Nanoscale* **2018**, *10*, 19766.
[17] J.-Y. Kim, W. Lee, Y. H. Kang, S. Y. Cho, K.-S. Jan, *Carbon* **2018**, *133*, 293.
[18] S. Yu, X. Wang, H. Xiang, L. Zhu, M. Tebyetekerwa, M. Zhu, *Carbon* **2018**, *140*, 1.
[19] L. Maillaud, R. J. Headrick, V. Jamali, J. Maillaud, D. E. Tsentalovich, W. Neri, E. A. Bengio, F. Mirri, O. Kleinerman, Y. Talmon, P. Poulin, M. Pasquali, *Ind. Eng. Chem. Res.* **2018**, *57*, 3554.
[20] X. Wu, X. K. Mukai, K. Asaka, T. Morimoto, T. Okazaki, *App. Phys. Express* **2017**, *10*, 055101.
[21] Z. Jiang, D. Chen, Y. Yu, J. Miao, Y. Liu, L. Zhang, *RSC Adv.* **2017**, *7*, 2186.
[22] T.-W. Lee, M. Han, S.-E. Lee, Y. G. Jeong, *Compos. Sci. Technol.* **2016**, *123*, 57.
[23] K. Mukai, K. Asaka, X. Wu, T. Morimoto, T. Okazaki, T. Saito, M. Yumura, *App. Phys. Express* **2016**, *9*, 055101.
[24] Y. Ma, P. Li, J. W. Sedloff, X. Zhang, H. Zhang, J. Liu, *ACS Nano* **2015**, *9*, 1352.
[25] C. Zhu, J. Chen, K. K. Koziol, J. W. Gilman, P. C. Trulove, S. S. Rahatekar, *eXPRESS Polym. Lett.* **2014**, *8*, 154.
[26] G. Park, Y. Jung, G.-W. Lee, J. P. Hinestroza, Y. Jeong, *Fibers Polym.* **2012**, *13*, 874.
[27] V. Sa, K. G. Kornev, *Carbon* **2011**, *49*, 1859.
[28] C. Mercader, V. D. Lutard, S. Jestin, M. Maugey, A. Derre, C. Zakri, P. Poulin, *J. App. Polym. Sci.* **2012**, *125*, E191.
[29] S. Zhang, K. K. K. Koziol, I. A. Kinloch, A. H. Windle, *Small* **2008**, *4*, 1217.
[30] J. M. Razal, K. J. Gilmore, G. G. Wallace, *Adv. Funct. Mater.* **2008**, *18*, 61.
[31] A. B. Dalton, S. Collins, J. Razal, E. Munoz, V. H. Ebron, B. G. Kim, J. N. Coleman, J. P. Ferraris, R. H. Baughman, *J. Mater. Chem.* **2004**, *14*, 1.
[32] N. T. Alvarez, P. Miller, M. R. Haase, R. Lobo, R. Malik, V. Shanov, *Carbon* **2019**, *144*, 55.
[33] Y. Dini, J. F. Vincent, J. Dijon, *Carbon* **2019**, *144*, 301.
[34] M. Han, J.-K. Kim, Y. Choi, J. P. Yun, G. S. Lee, S. W. Kang, D. Jung, *Jpn. J. App. Phys.* **2019**, *58*, SDDJ07.
[35] T. H. Nam, K. Goto, Y. Shimamura, Y. Inoue, S. Ogihara, *Adv. Compos. Mater.* **2019**, *28*, 507.
[36] S. N. Kanakaraj, N. T. Alvarez, S. Gbordzoe, M. S. Lucas, B. Maruyama, R. Noga, Y. Y. Hsieh, V. Shanov, *Mater. Res. Express* **2018**, *5*, 065036.
[37] J. Zhao, X. Zhang, Y. Huang, J. Zou, T. Liu, N. Liang, F. Yu, Z. Pan, Y. Zhu, M. Miao, *Mater. Des.* **2018**, *146*, 20.
[38] P. Wang, J. Yang, G. Sun, X. Zhang, H. Zhang, Y. Zheng, S. Xu, *Int. J. Plasticity* **2018**, *110*, 74.
[39] L. Qiu, H. Zou, N. Zhu, Y. Feng, X. Zhang, X. Zhang, *App. Thermal Eng.* **2018**, *141*, 913.
[40] P. Wang, D. Liu, J. Zou, Y. Ye, L. Hou, J. Zhao, C. Men, X. Zhang, Q. Li, *Mater. Des.* **2018**, *159*, 138.
[41] X. Zhang, L. Yang, H. Liu, *App. Phys. Lett.* **2018**, *112*, 164103.
[42] J.-G. Kim, H. Kang, Y. Lee, J. Park, J. Kim, T. Truong, E. S. Kim, D. H. Yoon, Y. H. Lee, D. Suh, *Adv. Funct. Mater.* **2017**, *27*, 1701108.
[43] Y. Zhang, G. Sun, Z. Zhan, L. Zheng, *J. Mater. Sci.* **2017**, *52*, 6196.
[44] N. T. Alvarez, P. Miller, M. Haase, N. Kienzle, L. Zhang, M. J. Schulz, V. Shanov, *Carbon* **2015**, *86*, 350.
[45] J. Jia, J. Zhao, G. Xu, J. Di, Z. Yong, Y. Tao, C. Fang, Z. Zhang, X. Zhang, L. Zheng, Q. Li, *Carbon* **2011**, *49*, 1333.
[46] M. Miao, *Carbon* **2011**, *49*, 3755.
[47] K. Liu, Y. Sun, R. Zhou, H. Zhu, J. Wang, L. Liu, S. Fan, K. Jiang, *Nanotechnology* **2010**, *21*, 045708.
[48] C. P. Huynh, S. C. Hawkins, *Carbon* **2010**, *48*, 1105.
[49] S. Zhang, L. Zhu, M. L. Minus, H. G. Chae, U. Jagannathan, C.-P. Wong, J. Kowalik, L. B. Roberson, S. Kumar, *J. Mater. Sci.* **2008**, *43*, 4356.
[50] X. Zhang, Q. Li, Y. Tu, Y. Li, J. Y. Coulter, L. Zheng, Y. Zhao, Q. Jia, D. E. Peterson, Y. Zhu, *Small* **2007**, *3*, 244.
[51] X. Zhang, Q. Li, T. G. Holesinger, P. N. Arendt, J. Huang, D. Kirven, T. G. Clapp, R. F. DePaula, X. Liao, Y. Zhao, L. Zheng, D. E. Peterson, Y. Zhu, *Adv. Mater.* **2007**, *19*, 4198.
[52] X. Zhang, K. Jiang, C. Feng, P. Liu, L. Zhang, J. Kong, T. Zhang, Q. Li, S. Fan, *Adv. Mater.* **2006**, *18*, 1505.

[53] Q. Li, X. Zhang, R. F. DePaula, L. Zheng, Y. Zhao, L. Stan, T. G. Holesinger, P. N. Arendt, D. E. Peterson, Y. T. Zhu, *Adv. Mater.* **2006**, *18*, 3160.
[54] M. Zhang, K. R. Atkinson, R. H. Baughman, *Science* **2004**, *306*, 1358.
[55] X. Rodiles, V. Reguero, M. Vila, B. Aleman, F. Arevalo, V. Fresno, D.-L. P. O'Shea, J. J. Vilatela, *Sci. Rep.* **2019**, *9*, 9239.
[56] B. Aleman, J. J. Vilatela, *Carbon* **2019**, *149*, 512.
[57] L. Weller, F. R. Smail, J. A. Elliott, A. H. Windle, A. M. Boies, S. Hochgreb, *Carbon* **2019**, *146*, 789.
[58] D. Lglesias, E. Senokos, B. Aleman, L. Cabana, C. Navio, R. Marcilla, M. Prato, J. J. Vilatela, S. Marchesan, *ACS App. Mater. Interfaces* **2018**, *10*, 5760.
[59] H. Khoshnevis, T. Q. Tran, S. M. Mint, A. Zadhoush, H. M. Duong, M. Youssefi, *Colloids Surf., A* **2018**, *558*, 570.
[60] L. Zheng, Y. Wang, J. Qin, X. Wang, R. Lu, C. Qu, C. Wang, *Vacuum* **2018**, *152*, 84.
[61] S.-H. Lee, H.-R. Kim, T. Lee, H. Lee, J. Lee, J. Lee, J. Park, K.-H. Lee, *Carbon* **2017**, *124*, 219.
[62] P. Liu, Y. Li, Y. Xu, L. Bao, L. Wang, J. Pan, Z. Zhang, X. Sun, H. Peng, *Small* **2018**, *14*, 1702926.
[63] T. Q. Tran, Z. Fan, P. Liu, S. M. Myint, H. M. Duong, *Carbon* **2016**, *99*, 407.
[64] J. Liu, W. Gong, Y. Yao, Q. Li, J. Jiang, Y. Wang, G. Zhou, S. Qu, W. Lu, *Compos. Sci. Technol.* **2018**, *164*, 290.
[65] B. Aleman, M. Vila, J. J. Vilatela, *Phys. Status Solidi A* **2018**, *215*, 1800187.
[66] S.-H. Lee, H.-R. Kim, H. Lee, J. Lee, C.-H. Lee, J. Lee, J. Park, H.-H. Lee, *Chem. Eng. Sci.* **2018**, *192*, 655.
[67] O. Aberefa, K. Bedasie, M. O. Daramola, S. E. Lyuke, *Adv. Nat. Sci.: Nanosci. Nanotechnol.* **2018**, *9*, 035009.
[68] G. Hou, D. Chauhan, V. Ng, C. Xu, Z. Yin, M. Paine, R. Su, V. Shanov, D. Mast, M. Schulz, Y. Liu, *Mater. Des.* **2017**, *132*, 112.
[69] A. Pendashteh, E. Senokos, J. Palma, M. Anderson, J. J. Vilatela, R. Marcilla, *J. Power Sources* **2017**, *372*, 64.
[70] R. M. Sundaram, A. H. Windle, *Mater. Des.* **2017**, *126*, 85.
[71] B. Mas, B. Aleman, I. Dopico, I. M. Bragado, T. Naranjo, E. M. Perez, J. J. Vilatela, *Carbon* **2016**, *101*,458.
[72] G. Hou, R. Su, A. Wang, V. Ng, W. Li, Y. Song, L. Zhang, M. Sundaram, V. Shanov, D. Mast, D. Lashmore, M. Schulz, Y. Liu, *Carbon* **2016**, *102*, 513.
[73] C. Paukner, K. K. K. Koziol, *Sci. Rep.* **2015**, *4*, 3903.
[74] V. Reguero, B. Aleman, B. Mas, J. J. Vilatela, *Chem. Mater.* **2014**, *26*, 3550.
[75] T. S. Gspann, F. Smail, A. H. Windle, *Faraday Discuss.* **2014**, *173*, 47.
[76] X.-H. Zhong, Y.-L. Li, J.-M. Feng, Y.-R. Kang, S.-S. Han, *Nanoscale* **2012**, *4*, 5614.
[77] J. J. Vilatela, L. Deng, I. Kinloch, R. J. Young, A. H. Windle, *Carbon* **2011**, *49*, 4149.
[78] R. M. Sundaram, K. K. K. Koziol, A. H. Windle, *Adv. Mater.* **2011**, *23*, 5064.
[79] J. J. Vilatela, A. H. Windle, *Adv. Mater.* **2010**, *22*, 4959.
[80] X.-H. Zhong, Y.-L. Li, Y.-K. Liu, X.-H. Qiao, Y. Feng, J. Liang, J. Jin, L. Zhu, F. Hou, J.-Y. Li, *Adv. Mater.* **2010**, *22*, 692.
[81] D. Conroy, A. Moisala, S. Cardoso, A. Windle, J. Davidson, *Chemical Eng. Sci.* **2010**, *65*, 2965.
[82] K. Koziol, J. Vilatela, A. Moisala, M. Motta, P. Cunniff, M. Sennett, A. Windle, *Science* **2007**, *318*, 1892.
[83] M. Motta, I. Kinloch, A. Moisala, V. Premnath, M. Pick, A. Windle, *Physica E* **2007**, *37*, 40.
[84] M. Motta, A. Moisala, I. A. Kinloch, A. H. Windle, *Adv. Mater.* **2007**, *19*, 3721.
[85] M. Motta, Y.-L. Li, I. Kinloch, A. Windle, *Nano Lett.* **2005**, *5*, 1529.
[86] Y.-L. Li, I. A. Kinloch, A. H. Windle, *Science* **2004**, *304*, 276.
[87] H. W. Zhu, C. L. Xu, D. H. Wu, B. Q. Wei, R. Vajtai, P. M. Ajayan, *Science* **2002**, *296*, 884.
[88] N. Behabtu, M. J. Green, M. Pasquali, *Nano Today* **2008**, *3*, 24.
[89] F. Cesano, M. J. Uddin, K. Lozano, M. Zanetti, D. Scarano, *Front. Mater.* **2020**, *7*, 219.
[90] G. Sun, X. Wang, P. Chen, *Mater. Today* **2015**, *18*, 215.
[91] A. Lekawa-Raus, J. Patmore, L. Kurzepa, J. Bulmer, K. Koziol, *Adv. Funct. Mater.* **2014**, *24*, 3661.
[92] W. Lu, M. Zu, J.-H. Byun, B.-S. Kim, T.-W. Chou, *Adv. Mater.* **2012**, *24*, 1805.
[93] L. Liu, W. Ma, Z. Zhang, *Small* **2011**, *11*, 1504.
[94] C. Subramaniam, T. Yamada, K. Kobashi, A. Sekiguchi, D. N. Futaba, M. Yumura, K. Hata, *Nat. Commun.* **2013**, *4*, 2202.
[95] G. J. Wang, Y. J. Ma, Y. P. Cai, Z. H. Cao, X. K. Meng, *Carbon* **2019**, *146*, 293.
[96] B. Han, E. Guo, X. Xu, Z. Zhao, L. Luo, H. Qu, T. Niu, Y. Xu, H. Hou, *Carbon* **2017**, *123*, 593.
[97] B. Han, E. Guo, X. Xu, Z. Zhao, T. Li, Y. Xu, L. Luo, H. Hou, *Appl. Surface Sci.* **2018**, *441*, 984.
[98] R. Sundaram, T. Yamada, K. Hata, A. Sekiguchi, *Sci. Rep.* **2017**, *7*, 9267.
[99] R. Sundaram, T. Yamada, K. Hata, A. Sekiguchi, *Mater. Today Commun.* **2017**, *13*, 119.
[100] R. Sundaram, T. Yamada, K. Hata, A. Sekiguchi, *Jpn. J. Appl. Phys.* **2018**, *57*, 04FP08.
[101] L. R. Randeniya, A. Bendavid, P. J. Martin, C.-D. Tran, *Small* **2010**, *6*, 1806.
[102] G. Xu, J. Zhao, S. Li, X. Zhang, Z. Yong, Q. Li, *Nanoscale* **2011**, *3*, 4215.
[103] Y. Feng, G. E. McGuire, O. A. Shenderova, H. Ke, S. L. Burkett, *Thin Solid Films* **2016**, *615*, 116.
[104] C. L. P. Pavithra, B. V. Sarada, K. V. Rajulapati, T. N. Rao, G. A. Sundararajan, *Sci. Rep.* **2014**, *4*, 4049.
[105] S. Arai, Y. Suwa, M. Endo, *J.Electrochem. Soc.* **2011**, *158*, D49.
[106] M.-Y. Cheng, K.-Y. Chen, T.-F. Liu, Y.-L.Wang , H.-P. Feng, *Thin Solid Films* **2010**, *518*, 7468.
[107] A. Aziz, M. B. Bazbouz, M. E. Welland, *ACS Appl. Nano Mater.* **2020**, *3*, 9385.
[108] P. G. Karagiannidis, S. A. Hodge, L. Lombardi, F. Tomarchio, N. Decorde, S. Milana, I. Goykhman, Y. Su, S. V. Mesite, D. N. Johnstone, R. K. Leary, P. A. Midgley, N. M. Pugno, F. Torrisi, A. C. Ferrari, *ACS Nano* **2017**, *11*, 2742.
[109] S. Luo, T. Liu, Y. Wang, L. Li, G. Wang, Y. Luo, *J. Nanoparticle Res.* **2016**, *18*, 243.
[110] S. Azoubel, S. Magdassi, *Carbon* **2010**, *48*, 3346.
[111] M. N. Nadagouda, R. S. Varma, *Macromol. Rapid Commun.* **2008**, *29*, 155.
[112] M. M. Hamedi, A. Hajian, A. B. Fall, K. Hakansson, M. Salajkova, F. Lundell, L. Wagberg, L. A. Berglund, *ACS Nano* **2014**, *8*, 2467.
[113] M. Nadler, T. Mahrholz, U. Riedel, C. Schilde, A. Kwade, *Carbon* **2008**, *46*, 1384.
[114] Q. Ouyang, Y.-S. Chen, N. Zhang, G.-M. Mo, D.-H. Li, Q. Yan, *J. Macromol. Sci., Part B: Phys.* **2011**, *50*, 2417.
[115] D. Grujicic, B. Pesic, *Electrochim. Acta* **2002**, *47*, 2901.
[116] M. B. Bazbouz, S. J. Russell, *J. Mater. Sci.* **2018**, *53*, 10891.
[117] W. Li, L. Liu, C. Zhong, B. Shen, W. Hu, *J. Alloys Compd.* **2011**, *509*, 3532.
[118] B. A. Kakade, V. K. Pillai, *Appl. Surface Sci.* **2008**, *254*, 4936.
[119] Y. Wang, Z. Iqbal, S. Mitra, *J. Am. Chem. Soc.* **2006**, *128*, 95.
[120] F. Aviles, J. V. Cauich-Rodriguez, L. Moo-Tah, A. May-Pat, R. Vargas-Coronado, *Carbon* **2009**, *47*, 2970.
[121] Y. Wei, X. Ling, L. Zou, D. Lai, H. Lu, Y. Xu, *Colloids Surf., A* **2015**, *482*, 507.
[122] L. Lu, Y. F. Shen, X. H. Chen, L. H. Qian, K. Lu, *Science* **2004**, *304*, 422.
[123] X. H. Zhong, R. Wang, Y. Y. Wen, *Phys. Chem. Chem. Phys.* **2013**, *15*, 3861.
[124] F. Gao, J. Qu, M. Yao, *Appl. Phys. Lett.* **2010**, *96*, 102108.

[125] M. Ghorbani-Asl, P. D. Bristowe, K. Koziol, *Phys. Chem. Chem. Phys.* **2015**, *17*, 18273.
[126] G. Mokry, J. Pozuelo, J. J. Vilatela, J. Sanz, J. Baselga, *Nanomaterials* **2019**, *9*, 383.
[127] A. Kamyshny, S. Magdassi, *Chem. Soc. Rev.* **2019**, *48*, 1712.
[128] A. Kamyshny, S. Magdassi, *Small* **2014**, *10*, 3515.
[129] X. Wang, N. Behabtu, C. C. Young, D. E. Tsentalovich, M. Pasquali, J. Kono, *Adv. Funct. Mater.* **2014**, *24*, 3241.
[130] D. B. Butrymowicz, J. R. Manning, M. E. Read, *J. Phys. Chem. Ref. Data* **1973**, *2*, 643.
[131] P. Kim, L. Shi, A. Majumdar, P. L. McEuen, *Phys. Rev. Lett.* **2001**, *87*, 215502.